Álvarez Polegre, A., Riera-Palou, F., Femenias, G. & García Armada, A. (07-11 June 2020). *New insights on channel hardening in cell-free massive MIMO networks* [proceedings]. 2020 IEEE International Conference on Communications Workshops (ICC Workshops), Dublin, Ireland.

DOI: 10.1109/ICCWorkshops49005.2020.9145215

New Insights on Channel Hardening in Cell-Free Massive MIMO Networks

Alberto Álvarez Polegre*, Felip Riera-Palou†, Guillem Femenias†, Ana García Armada*
aalvarez@tsc.uc3m.es, felip.riera@uib.cat, guillem.femenias@uib.cat, agarcia@tsc.uc3m.es
*Deparment of Signal Theory and Communications, Universidad Carlos III de Madrid
†Mobile Communications Group, Universitat de les Illes Balears

***Abstract*—The cell-free (CF) massive multiple-input multiple-output (M-MIMO) architecture has recently emerged as a key technology for future wireless networks that is shown to outperform alternative network deployments such as those based on small-cells. Despite the many characteristics CF-M-MIMO shares with conventional M-MIMO (i.e., centralized) systems, its distributed nature brings along new issues that need to be carefully accounted for. In particular, the so-called channel hardening effect that postulates that the variance of the compound wireless channel experienced by a given user from a large number of transmit antennas tends to vanish, effectively making the channel deterministic. This critical assumption, which permeates most theoretical results of M-MIMO, has been well investigated and validated in centralized architectures, however, it has received little attention in the context of CF-M-MIMO networks. Hardening in CF-M-MIMO is potentially compromised by the different large-scale gains each access point (AP) impinges to the transmitted signal to each user, a condition that is further stressed when not all APs transmit to all users as proposed in the user-centric (UC) variations of CF-M-MIMO. This paper aims at presenting a comprehensive study of the channel-hardening effect in CF-M-MIMO under realistic operational conditions (e.g, presence of pilot contamination, power control, different precoders). Closed-form expressions of the hardening coefficient for different precoding schemes are provided showing that the precoder's choice, the number of antennas at each AP and the geographical density of APs play a key role in achieving this property.**

***Index Terms*—Cell-Free, Channel Hardening, User-Centric, Massive MIMO**

I. Introduction

Base station coordination has been taken one step further with cell-free massive multiple-input multiple-output (CF-M-MIMO) [1], where a large number of low-power access points (APs) serve in a coordinated manner a much smaller number of mobile stations (MSs), effectively resulting in a distributed massive MIMO (M-MIMO) system. CF-M-MIMO architectures avoid the formation of cells, thus eliminating edge performance issues, while taking the network infrastructure physically closer to the MSs. In the original proposal, a single central processing unit (CPU) is used to coordinate all APs that transmit to all users over the same time-frequency resource relying on time-division duplex (TDD), as is commonly done in co-located massive MIMO systems [2]. Recently, the user-centric (UC) approach to CF-M-MIMO has been proposed in [3] whereby each AP only serves a subset of users. The criterion for selecting the set of users served by a given AP is mostly based on transmitting to those users showing the best channel propagation conditions with respect to that particular AP. As shown in [4], the UC approach has lower fronthaul requirements than a fully-fledged CF architecture at the cost of a modest performance penalty.

The theoretical underpinnings of CF-M-MIMO borrow many results from the centralized M-MIMO literature. Notably, in the context of M-MIMO, closed-form expressions for achievable rates have been found that, under the assumption of channel hardening, are shown to tightly lower-bound the corresponding true rates when employing simple, yet extremely effective, precoding schemes such as conjugate beamforming (CB) [5]. Moreover, the presence of channel hardening renders the downlink channel estimation unnecessary since the channel tends to become deterministic. Furthermore, these theoretical rate expressions are found to depend only on large-scale channel statistics and therefore can be used as the objective functions driving the optimization procedures to suitably determine the power coefficients and/or pilot sequence allocation. Parallelizing their centralized M-MIMO counterparts, closed-form expressions for the achievable rate were presented in [1] for the case of CF-M-MIMO. The distributed nature of CF-M-MIMO, with APs inducing different large-scale fading coefficients with respect to a given user, may compromise the channel hardening, causing the achievable rate bounds to significantly underestimate the true performance of the system. In [6] an extensive analytical framework based on stochastic geometry when considering CB precoding is introduced that actually questions the hardening effect in CF-M-MIMO, specially when APs are single-antenna. Nonetheless, authors in [6], for the sake of analytical tractability, assume the absence of pilot contamination, the availability of perfect channel state information (CSI) at the APs and also neglect any effect induced by the power control coefficients or the use of more sophisticated precoding strategies.

The main aim of this paper is to revisit the channel hardening hypothesis taking into account operational conditions that are often met in practice. In particular, the contributions are:

1) Closed-forms expressions for the hardening coefficient are provided when considering minimum mean-square error (MMSE) channel estimation, pilot contamination and power loading. The hardening effects are then contrasted with curves obtained for the achievable and true rates of the network that serve to assess under what conditions is hardening actually achieved.
2) The hardening coefficient is also evaluated when using the normalized conjugate beamforming (NCB) introduced in [7], a precoder designed to satisfy short-term power constraints and that, as it is shown in this work, leads to a large advantage in terms of hardening with respect to CB. Remarkably, novel analytical expressions for the achievable rate are derived. Note that the original

NCB proposal was limited to single-antenna APs. In this work we propose and analyze the vector-NCB.

3) Channel hardening is finally revisited in the context of UC architectures for both CB and NCB precoding.

II. System Model

Let us consider a large coverage area where K single-antenna MSs and M APs are randomly deployed according to a uniform distribution. APs are assumed to be equipped with an array of N antennas. Transmissions are organized in a TDD operation whereby each coherence time interval is divided into three phases: uplink pilots training, downlink data transmission and uplink data transmission. For ease of presentation, this paper focuses on the performance of the downlink communication segment.

A. Channel model

We model the channel between the m-th AP and the k-th MS as an $N \times 1$ vector,

$$\boldsymbol{g}_{mk} = \sqrt{\beta_{mk}}\boldsymbol{h}_{mk}, \tag{1}$$

with $\boldsymbol{h}_{mk} \sim \mathcal{CN}(0, \boldsymbol{I}_N)$ representing the small-scale fading and β_{mk} being a scalar value representing the large-scale fading. For later convenience we denote $\boldsymbol{g}_k = [\boldsymbol{g}_{1k}^T \dots \boldsymbol{g}_{Mk}^T]^T$ as the channel vector between the k-th MS and all APs. Large-scale coefficients are expressed as $\beta_{mk} = \zeta_{mk}\chi_{mk}$ with

$$\zeta_{mk}[\text{dB}] = -30 - 36.7\log_{10}(d_{mk}), \tag{2}$$

representing the distance-dependent path loss with d_{mk} being the distance between the m-th AP and the k-th MS expressed in m. The 3-slope path loss model previously used in [1] is actually based on macro-cell deployments and could lead to inaccurate conclusions, while (2) matches better micro-cell scenarios [8]. The shadowing component χ_{mk} is modeled as a correlated log-normal random variable with variance σ_χ^2 whose spatial correlation model is described in [1, (54)-(55)].

B. Channel Estimation

During the training phase, comprising τ_p time/frequency samples, pilots are sent from MSs to APs in order to perform channel estimation. The $N \times \tau_p$ received training signal at the m-th AP is

$$\boldsymbol{Y}_m = \sqrt{\rho_u \tau_p}\sum_{k=1}^{K}\boldsymbol{g}_{mk}\boldsymbol{\varphi}_k^T + \boldsymbol{W}_m, \tag{3}$$

where ρ_u is the uplink normalized signal-to-noise ratio (SNR), $\boldsymbol{\varphi}_k$ is the $\tau_p \times 1$ k-th user training sequence with $\|\boldsymbol{\varphi}_k\|^2 = 1$ and $\boldsymbol{W}_m$ is a $N \times \tau_p$ matrix of independent and identically distributed (i.i.d.) additive noise samples with each entry distributed as $\mathcal{CN}(0,1)$.

In order to perform the uplink channel estimation, a pilot assignment strategy needs to be carried out whereby each user is assigned a specific training sequence. Note that τ_p is assumed to be considerably shorter than the communication coherence time/frequency interval (τ_c). Assuming that the length of the available orthogonal pilots is equal to τ_p, two different situations are considered:

1) *Orthogonal pilot assignment*: For a low number of users, i.e. $K \leq \tau_p$, every MS is assigned a fully orthogonal pilot, thus avoiding pilot contamination.

2) *Fingerprinting pilot assignment*: In those cases where the number of users is greater than the length of the training sequence, i.e. $K > \tau_p$, pilot reuse will bring along pilot contamination. In this paper, we employ the fingerprinting pilot assignment first proposed in [9]. This particular strategy ensures that a pilot sequence will only be reused by those users showing the highest dissimilarity in terms of their large-scale channel coefficients.

Channel estimates are obtained at the APs using the MMSE estimator, which requires knowledge of the large-scale fading coefficients β_{mk}. These coefficients are considered to remain static during several channel coherence intervals and known perfectly beforehand [2]. Under this assumption, the channel estimate using MMSE is

$$\hat{\boldsymbol{g}}_{mk} = \frac{\sqrt{\rho_u\tau_p}\beta_{mk}}{\rho_u\tau_p\sum\limits_{k'=1}^{K}\beta_{mk'}\left|\boldsymbol{\varphi}_k^H\boldsymbol{\varphi}_{k'}\right|^2 + 1}\boldsymbol{Y}_m\boldsymbol{\varphi}_k^*, \tag{4}$$

whose entries are distributed as $\mathcal{CN}(0, \gamma_{mk})$ with

$$\gamma_{mk} = \frac{\rho_u\tau_p\beta_{mk}^2}{\rho_u\tau_p\sum\limits_{k'=1}^{K}\beta_{mk'}\left|\boldsymbol{\varphi}_k^H\boldsymbol{\varphi}_{k'}\right|^2 + 1}, \tag{5}$$

corresponding to the mean square of the channel estimates. In addition, and owing to the use of distributed precoding strategies described later, CSI is neither sent back to the CPU nor exchanged among APs reducing in this way the fronthaul overhead. The channel estimation error, $\boldsymbol{\epsilon}_{mk} = \boldsymbol{g}_{mk} - \hat{\boldsymbol{g}}_{mk}$, has i.i.d. entries distributed as $\mathcal{CN}(0, \beta_{mk} - \gamma_{mk})$ [1].

III. Downlink Signal Processing

As stated before, in the UC approach only a subset of MSs are served by the m-th AP. Each AP provides service to the K_{UC} users exhibiting the strongest channel gain (largest β_{mk}). In order to generalize the model regarding the followed architecture, we use the connectivity matrix $\boldsymbol{C}$ introduced in [4], whose components are described as

$$c_{mk} = \begin{cases} 1, & \text{if the } m\text{-th AP serves the } k\text{-th MS,} \\ 0, & \text{otherwise.} \end{cases} \tag{6}$$

The classical CF scheme results when $c_{mk} = 1\ \forall m, k$. Note that alternative selection strategies can be derived by properly selecting the entries in $\boldsymbol{C}$ without affecting the subsequent analysis presented in the following sections.

A. Precoding Schemes and Power Allocation Strategies

In this work the multi-antenna AP version of the precoding scheme CB [1] and NCB [7] are employed, which are defined as

$$\boldsymbol{\varpi}_{mk}^{\text{CB}} = c_{mk}\sqrt{\eta_{mk}}\hat{\boldsymbol{g}}_{mk}^H, \tag{7}$$

and

$$\boldsymbol{\varpi}_{mk}^{\text{NCB}} = c_{mk}\sqrt{\eta_{mk}}\frac{\hat{\boldsymbol{g}}_{mk}^H}{\|\hat{\boldsymbol{g}}_{mk}\|_2}, \tag{8}$$

respectively, where η_{mk} is the power coefficient assigned to the link between the k-th MS and the m-th AP. If we define

$$z_{mk} \triangleq \mathbb{E}\left\{\|\hat{\boldsymbol{g}}_{mk}\|_2\right\} = \mathbb{E}\left\{\sqrt{\sum_{n=1}^{N}|\hat{g}_{mkn}|^2}\right\}, \tag{9}$$

being $\hat{g}_{mkn}$ the n-th entry of $\hat{\boldsymbol{g}}_{mk}$, then

$$\mathbb{E}\{z_{mk}\} = \frac{2}{\Gamma(N)\gamma_{mk}^N}\int_0^\infty z^{2N}e^{-z^2/\gamma_{mk}}dz = \frac{\Gamma(N+1/2)}{\Gamma(N)}\sqrt{\gamma_{mk}}. \quad (10)$$

For later convenience we define $\Gamma_N \triangleq \frac{\Gamma(N+1/2)}{\Gamma(N)}$.

The downlink payload signal results in

$$\boldsymbol{x}_m = \sqrt{\rho_d}\sum_{k=1}^{K}\boldsymbol{\varpi}_{mk}^a s_k, \quad (11)$$

where ρ_d is the normalized downlink SNR, s_k is the data symbol intended for the k-th user, with $\mathbb{E}\left\{|s_k|^2\right\}=1$, and a is a token being either CB or NCB. For convenience we denote $\boldsymbol{\varpi}_k^a = [\boldsymbol{\varpi}_{1k}^a \ldots \boldsymbol{\varpi}_{Mk}^a]$ as the precoding vector between the k-th MS and all APs. The power coefficients are designed to fulfill the average power constraint

$$\mathbb{E}\left\{\|\boldsymbol{x}_m\|^2\right\} \le \rho_d. \quad (12)$$

The power control strategy is precoder-dependent. A uniform power control scheme has been proven to be well matched to the CB precoding [10], while NCB precoding best suits a power allocation strategy where MSs with strongest channels are assigned more power [7]. These coefficients are then expressed as

$$\eta_{mk} = \begin{cases} \frac{1}{N\sum_{k'=1}^{K} c_{mk'}\gamma_{mk'}}, & \text{CB}, \\ \frac{\gamma_{mk}}{\sum_{k'=1}^{K} c_{mk'}\gamma_{mk'}}, & \text{NCB}. \end{cases} \quad (13)$$

Note that other power allocation strategies (e.g. max-min fairness [1]) could be employed without compromising the analysis developed next.

B. Signal Reception and Achievable Rate

For single-antenna users, the received data signal at the k-th MS is given by

$$\hat{s}_k = \sum_{m=1}^{M}\boldsymbol{x}_m\boldsymbol{g}_{mk} + w_k = \sqrt{\rho_d}\sum_{m=1}^{M}\sum_{k'=1}^{K}\boldsymbol{\varpi}_{mk'}^a\boldsymbol{g}_{mk}s_{k'} + w_k, \quad (14)$$

where w_k is the receiver thermal noise modeled as a $\mathcal{CN}(0,\sigma_{w_k}^2)$ RV. Assuming that users only have statistical knowledge of the CSI, we may rewrite (14) as [1]

$$\hat{s}_k = \text{DS}_k^a s_k + \text{BU}_k^a s_k + \sum_{k'\neq k}^{K}\text{UI}_{kk'}^a s_{k'} + w_k, \quad (15)$$

where

$$\text{DS}_k^a = \sqrt{\rho_d}\,\mathbb{E}\left\{\sum_{m=1}^{M}\boldsymbol{\varpi}_{mk}^a\boldsymbol{g}_{mk}\right\}, \quad (16)$$

$$\text{BU}_k^a = \sqrt{\rho_d}\sum_{m=1}^{M}\left(\boldsymbol{\varpi}_{mk}^a\boldsymbol{g}_{mk} - \mathbb{E}\left\{\sum_{m=1}^{M}\boldsymbol{\varpi}_{mk}^a\boldsymbol{g}_{mk}\right\}\right), \quad (17)$$

and

$$\text{UI}_{kk'}^a = \sqrt{\rho_d}\sum_{m=1}^{M}\boldsymbol{\varpi}_{mk'}^a\boldsymbol{g}_{mk}, \quad (18)$$

represent the desired signal, the self-interference contribution due to the beamforming uncertainty and the multi-user interference, respectively. Now, a lower-bound achievable rate [2] for the k-th MS can be obtained as

$$R_k^{a,\text{LB}} = \bar{B}\log_2(1+\text{SINR}_k^a), \quad (19)$$

with

$$\bar{B} = B\frac{1-\tau_p/\tau_c}{2}, \quad (20)$$

where B is the system bandwidth, the term $1-\tau_p/\tau_c$ represents the losses due to training [1], while the factor $1/2$ accounts for the equal time division between uplink and downlink and

$$\text{SINR}_k^a = \frac{|\text{DS}_k^a|^2}{\mathbb{E}\{|\text{BU}_k^a|^2\} + \sum_{k'\neq k}^{K}\mathbb{E}\{|\text{UI}_{kk'}^a|^2\}+1}. \quad (21)$$

It is straightforward to extend this expression as in [1, (24)] to the multi-antenna APs case for the CB precoder [11], while the expressions for the NCB precoder are

$$|\text{DS}_k^{\text{NCB}}|^2 = \rho_d\left(\Gamma_N\sum_{m=1}^{M}c_{mk}\sqrt{\eta_{mk}\gamma_{mk}}\right)^2, \quad (22)$$

$$\mathbb{E}\left\{|\text{BU}_k^{\text{NCB}}|^2\right\} = \rho_d\sum_{m=1}^{M}c_{mk}\eta_{mk}\left(\beta_{mk} + \left(N-\Gamma_N^2-1\right)\gamma_{mk}\right), \quad (23)$$

and

$$\begin{aligned}\mathbb{E}\left\{|\text{UI}_{kk'}^{\text{NCB}}|^2\right\} &= \rho_d\sum_{m=1}^{M}c_{mk'}\eta_{mk'}\left(\beta_{mk} + (N-1)\gamma_{mk}\left|\boldsymbol{\varphi}_k^H\boldsymbol{\varphi}_{k'}\right|^2\right) \\ &\quad + \rho_d\sum_{m=1}^{M}\sum_{m'\neq m}^{M}c_{mk'}c_{m'k'} \\ &\quad \times\Gamma_N^2\sqrt{\eta_{mk'}\eta_{m'k'}\gamma_{mk}\gamma_{m'k}}\left|\boldsymbol{\varphi}_k^H\boldsymbol{\varphi}_{k'}\right|^2. \end{aligned} \quad (24)$$

Proofs are shown in Appendices A, B and C, respectively.

IV. Channel Hardening Metric

In co-located massive MIMO systems, when the number of transmitting antennas is large enough, the channel between an AP and a MS becomes quasi-deterministic [5] due to the channel hardening effect. Under such circumstances, there is no need for the user to estimate its instantaneous channel gain, but instead it can solely rely on channel statistics. For the specific case of CB and assuming perfect CSI at the APs, channel hardening can be mathematically expressed as [6]

$$\frac{\|\boldsymbol{h}_k\|^2}{\mathbb{E}\{\|\boldsymbol{h}_k\|^2\}} \longrightarrow 1, \text{ as } N\longrightarrow\infty, \quad (25)$$

with $\|\boldsymbol{h}_k\|^2$ representing the effective channel gain between the k-th user and all antennas from a particular AP [5]. In

words, the instantaneous equivalent channel converges to its mean when transmission takes place from a large number of co-located antennas. The channel hardening condition for CB or NCB can be more generally expressed as

$$\frac{|\boldsymbol{\varpi}_k^a \boldsymbol{g}_k|}{\mathbb{E}\left\{|\boldsymbol{\varpi}_k^a \boldsymbol{g}_k|\right\}} \longrightarrow 1, \text{ as } M, N \longrightarrow \infty, \tag{26}$$

whereby notice how, due to the definition of $\boldsymbol{\varpi}_k^a$, the effects of the power allocation, imperfect CSI and specific choice of precoder, are all now reflected in the hardening expression. Building on results in [6], the channel hardening metric can be re-expressed as

$$\begin{aligned}\xi_k^a &= \text{Var}\left\{\frac{|\boldsymbol{\varpi}_k^a \boldsymbol{g}_k|}{\mathbb{E}|\boldsymbol{\varpi}_k^a \boldsymbol{g}_k|}\right\} = \frac{\text{Var}\left\{|\boldsymbol{\varpi}_k^a \boldsymbol{g}_k|\right\}}{\mathbb{E}\{\boldsymbol{\varpi}_k^a \boldsymbol{g}_k\}^2} \\ &= \frac{\mathbb{E}\left\{|\boldsymbol{\varpi}_k^a \boldsymbol{g}_k|^2\right\} - \mathbb{E}\left\{|\boldsymbol{\varpi}_k^a \boldsymbol{g}_k|\right\}^2}{\mathbb{E}\left\{|\boldsymbol{\varpi}_k^a \boldsymbol{g}_k|\right\}^2} = \frac{\mathbb{E}\left\{|\text{BU}_k|^2\right\}}{|\text{DS}_k|^2}.\end{aligned} \tag{27}$$

The closed-form expression for (27), for any finite M and K, with CB precoding is given by

$$\xi_k^{\text{CB}} = \frac{\sum_{m=1}^{M} c_{mk}\eta_{mk}\gamma_{mk}\beta_{mk}}{N\left(\sum_{m=1}^{M} c_{mk}\sqrt{\eta_{mk}}\gamma_{mk}\right)^2}, \tag{28}$$

while for the NCB precoding is given by

$$\xi_k^{\text{NCB}} = \frac{\sum_{m=1}^{M} c_{mk}\eta_{mk}\left(\beta_{mk} + \left(N - \Gamma_N^2 - 1\right)\gamma_{mk}\right)}{\Gamma_N^2\left(\sum_{m=1}^{M} c_{mk}\sqrt{\eta_{mk}\gamma_{mk}}\right)^2}. \tag{29}$$

The computation of (28) can be easily proven using the analytical tools used in [1], whilst the computation for the NCB precoder follows directly from the results in the appendices.

The convergence of these ratios to 0 would imply that the instantaneous channel vector is close to its mean and thus a high degree of channel hardening is achieved. Having a low degree of channel hardening leads to a poor estimation of the achievable rate when using the lower-bound in (19). Therefore, in order to contrast the information provided by the hardening coefficient, we define a rate expression for a genie-aided user that perfectly knows its instantaneous channel gain as

$$R_k^{a,\text{GA}} = \bar{B}\mathbb{E}\left\{\log_2\left(1 + \frac{\sqrt{\rho_d}|\boldsymbol{\varpi}_k^a \boldsymbol{g}_k|^2}{\sum_{k' \neq k}^{K}\sqrt{\rho_d}|\boldsymbol{\varpi}_{k'}^a \boldsymbol{g}_k|^2 + 1}\right)\right\}. \tag{30}$$

This expression provides a benchmark against which the lower-bound achievable rate metrics can be measured. In those scenarios where hardening takes place, (19) and (30) should tend to match each other when the number of antennas and/or APs grow large. On the contrary, when hardening is compromised, the achievable rate provided by (19) can dramatically differ from the upper bound. In addition, it would underestimate the true rate a user can enjoy. Note, unfortunately, that (30) can only be estimated by simulation as it exhibits a dependence on the instantaneous CSI. Such a dependence precludes its practical use in governing power allocation or pilot assignment strategies that can be developed on the basis of achievable rate expressions. Consequently, it is desirable to establish conditions under which achievable rates are significantly close to the genie-aided user rates. We note that the gap between (19) and (30) also depends on the power allocation strategy since this has a large impact on the large-scale fading contribution that each user experiences. In distributed massive MIMO systems like CF, there is also a dependency on the path loss propagation model as well as the spatial density of APs, thus compromising the achievability of channel hardening [6]. It seems obvious that in the UC approach it would be even more difficult to achieve a high degree of channel hardening since there are less transmitting elements to a particular MS. Intuitively, the degree of channel hardening can be improved by increasing the spatial density of APs and/or the number of antenna elements in each AP.

V. Numerical Results

Similar to previous CF research, we consider for our experiments a squared coverage area with side $L = 1000$ m. In order to avoid boundary effects, a wrapping around technique is implemented [12]. The carrier frequency and system bandwidth are set to $f_c = 1.9$ GHz and $B = 20$ MHz, respectively. Each AP has $h_{\text{AP}} = 15$ m and a transmission power of $P_d = 200$ mW, while MSs have $h_{\text{MS}} = 1.65$ m and a transmission power of $P_u = 100$ mW. The shadow fading decorrelation distance has been set to $d_{\text{decorr}} = 50$ m. Receivers' noise figure is set to 9 dB. Channel coherence interval is assumed to be $\tau_c = 200$ samples in the time/frequency grid, while the training sequence duration is set to $\tau_p = 20$ samples.

A. Channel Hardening Ratio

The channel hardening ratio is depicted in Figs. 1 and 3 with power control, and in Figs. 2 and 4 without it, for different values of M using CB and NCB precoders, respectively. In agreement with [6], it is noticeable how for the single-antenna scenario under CB precoder, the hardening convergence is questionable, thus indicating that the true performance is likely to exceed the forecasted by the lower bound achievable rate. This would be the case experienced in most of the CF literature, specially in the seminal research works on this topic. However, by increasing the number of transmitting antennas at the APs, a much higher degree of hardening is achieved. Slight differences are shown between the CF and UC approaches, however having $N \neq 1$ and large M almost makes those differences negligible. These results confirm that equipping the APs with more antennas always helps the channel to harden and makes the lower-bound achievable rate expressions tighter regarding the upper bound. Confronting the results for CB with and without power control, it is worth noting that the power allocation coefficients significantly alter, in this case improves, the hardening metric. Assessing the impact other power allocation strategies may have on the hardening metric would be interesting for further research. Turning now the attention on the NCB precoder, the hardening ratio decreases considerably when compared to the

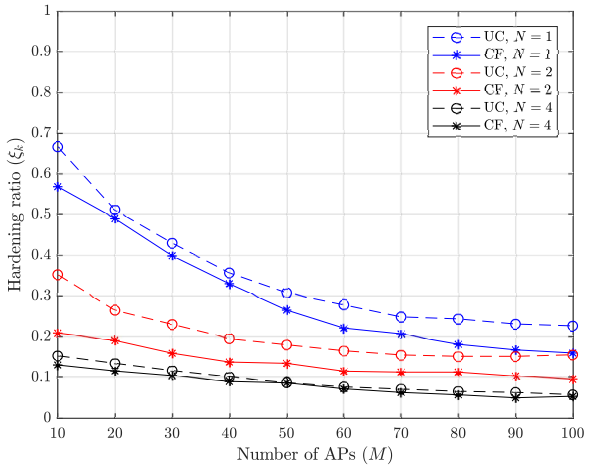

Fig. 1: Channel hardening ratio for $K = 10$ and different N under CF and UC ($K_{\text{UC}} = 5$) architectures with CB precoder with power control.

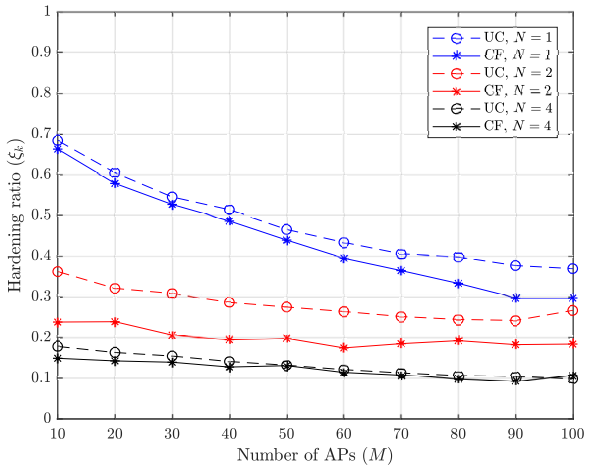

Fig. 2: Channel hardening ratio for $K = 10$ and different N under CF and UC ($K_{\text{UC}} = 5$) architectures with CB precoder without power control.

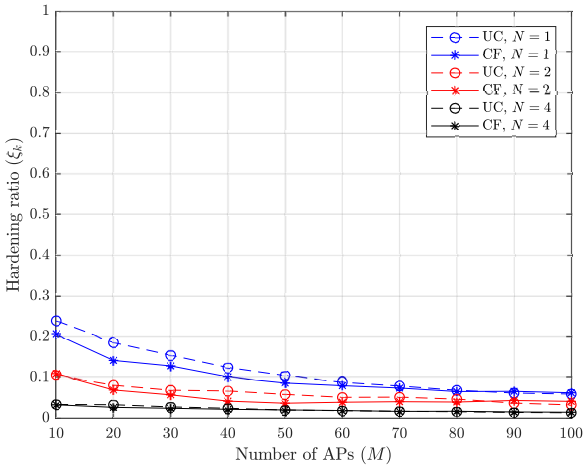

Fig. 3: Channel hardening ratio for $K = 10$ and different N under CF and UC ($K_{\text{UC}} = 5$) architectures with NCB precoder with power control.

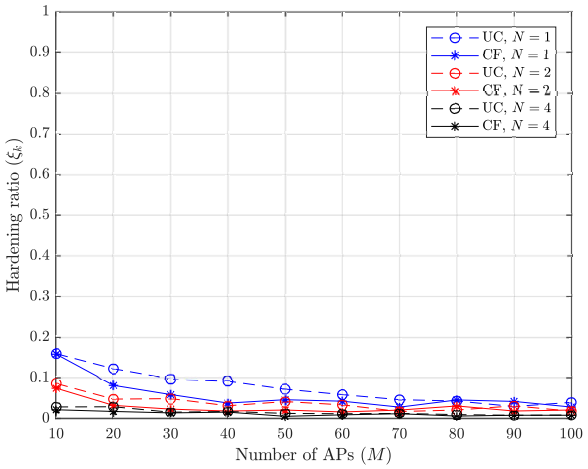

Fig. 4: Channel hardening ratio for $K = 10$ and different N under CF and UC ($K_{\text{UC}} = 5$) architectures with NCB precoder without power control.

CB precoder. This fact can be attributed to the normalization step NCB implements and suggests that NCB is a far more desirable precoding option than plain CB since it enforces APs to fulfill an instantaneous power constraint, it improves the hardening effect and, as it will be shown next, does not degrade the rate performance.

B. Lower-bound Achievable and Genie-aided Rates

A comparison between the lower-bound achievable rate and the genie-aided rate is shown in Figs. 5 and 7 for CB and NCB precoders, respectively. When having a large coverage area the gap between the two metrics is considerably high, while reducing this area makes the lower bound tighter, as Figs. 6 and 8 show. This trend is present for both precoders, though the gap when using the NCB precoder, as shown in Fig. 3, is smaller; in line with the lower channel hardening ratio NCB attains. In the case of the UC approach, the behavior is similar but with slightly worse performance (bear in mind that the original CF proposal constituted an upper bound in terms of average user rate). Increasing the number of antennas per AP entails reducing the hardening ratio and, thus, the gap between lower-bound and genie-aided rates. This fact can be observed in the relative difference between rates defined as $(R_k^{\text{GA}} - R_k^{\text{LB}})/R_k^{\text{GA}}$ for different values of N, which can be seen to decrease with increasing N. As an example, in Fig. 5 for the CF approach, the lower-bound and genie-aided rates gap for $N = 1$ is 37%, while for $N = 2$ is 31.9% and for $N = 4$ is 27.18%. Lastly, it is worth noting that the sudden reduction of rate in $L = 100$ m for both precoders when $K > 20$ is due to the pilot contamination ($K > \tau_p$). This drop is present for every L, however, it is much more pronounced when the area is small because of the close vicinity of users sharing the same pilot sequence.

VI. Conclusion

This paper has studied the channel hardening effect in CF-M-MIMO systems under realistic operational conditions. Closed-form expressions for the channel hardening coefficient

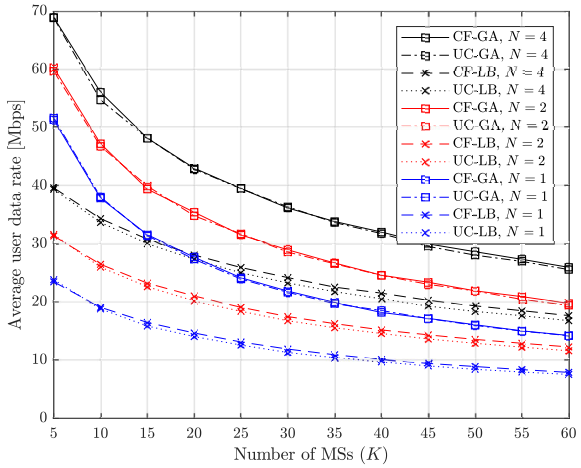

Fig. 5: Comparison between lowed-bound and genie-aided rates for $M = 100$ and $L = 1000$ m under CF and UC ($K_{\text{UC}} = 5$) architectures with CB precoder.

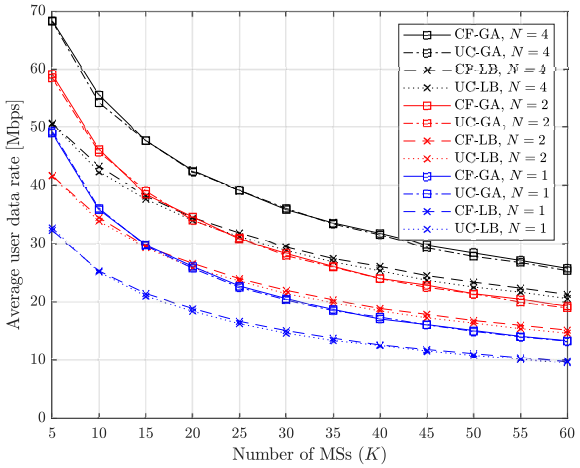

Fig. 7: Comparison between lowed-bound and genie-aided rates for $M = 100$ and $L = 1000$ m under CF and UC ($K_{\text{UC}} = 5$) architectures with NCB precoder.

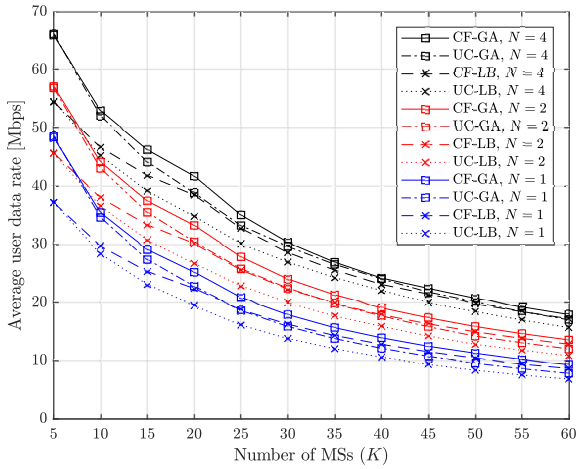

Fig. 6: Comparison between lowed-bound and genie-aided rates for $M = 100$ and $L = 100$ m under CF and UC ($K_{\text{UC}} = 5$) architectures with CB precoder.

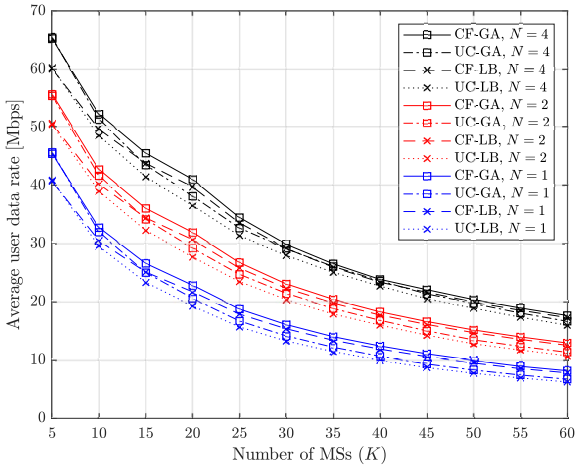

Fig. 8: Comparison between lowed-bound and genie-aided rates for $M = 100$ and $L = 100$ m under CF and UC ($K_{\text{UC}} = 5$) architectures with NCB precoder.

and achievable rates have been derived for the multi-antenna APs version of CB and vector NCB precoders when considering the use of imperfect CSI, pilot contamination and power loading. Numerical results have confirmed the advantage that the NCB precoder has over the CB scheme in terms of channel hardening. The effects of hardening in the recently proposed UC approach have also been investigated revealing a rather modest degradation, both, in achievable rate and hardening that becomes negligible as the number of APs and/or antennas per AP in the network increases. It has been shown that taking for granted the presence of channel hardening could lead to very poor estimation of the achievable rates, especially in large coverage areas with single-antenna APs. Future research will encompass centralized precoding schemes, such as zero-forcing (ZF) precoder, while also considering a more general channel model able to include the effects of spatial correlation at the APs and the existence of line-of-sight propagation (LOS). In addition, the uplink scenario may be considered.

ACKNOWLEDGEMENTS

Work supported by MINECO and FEDER under project TERESA (subprojects TEC2017-90093-C3-2-R and TEC2017-90093-C3-3-R), Spain.

APPENDIX

A. Computation of $|DS_k|^2$ with NCB precoding

$$
\begin{aligned}
|\mathrm{DS}_k|^2 &= \rho_d \mathbb{E}\left\{|\boldsymbol{\varpi}_k^{\text{NCB}} \boldsymbol{g}_k|\right\}^2 \\
&= \rho_d \left(c_{mk} \sqrt{\eta_{mk}} \mathbb{E}\left\{ \frac{\hat{\boldsymbol{g}}_{mk}^H}{\|\hat{\boldsymbol{g}}_{mk}\|_2} \boldsymbol{g}_{mk} \right\} \right)^2 \\
&= \rho_d \left(\sum_{m=1}^{M} c_{mk} \sqrt{\eta_{mk}} \mathbb{E}\left\{ \|\hat{\boldsymbol{g}}_{mk}^H\|_2 \right\} \right) \\
&= \rho_d \left(\Gamma_N \sum_{m=1}^{M} c_{mk} \sqrt{\eta_{mk} \gamma_{mk}} \right)^2 . \qquad (31)
\end{aligned}
$$

B. Computation of $\mathbb{E}\left\{|BU_k|^2\right\}$ with NCB precoding

$$\begin{aligned}
&\mathbb{E}\left\{ |\mathrm{BU}_k|^2\right\} \\
&= \rho_d \left(\mathbb{E}\left\{ |\boldsymbol{\varpi}_k^{\mathrm{NCB}} \boldsymbol{g}_k|^2 \right\} - \mathbb{E}\left\{ |\boldsymbol{\varpi}_k^{\mathrm{NCB}} \boldsymbol{g}_k| \right\}^2 \right) \\
&= \rho_d \Bigg(\sum_{m=1}^{M} \sum_{m'=1}^{M} c_{mk} c_{m'k} \sqrt{\eta_{mk}\eta_{m'k}} \\
&\quad \times \mathbb{E}\left\{ \frac{\hat{\boldsymbol{g}}_{mk}^H}{\|\hat{\boldsymbol{g}}_{mk}\|_2} \boldsymbol{g}_{mk} \boldsymbol{g}_{m'k}^H \frac{\hat{\boldsymbol{g}}_{m'k}}{\|\hat{\boldsymbol{g}}_{m'k}\|_2} \right\} \\
&\quad - \left(\Gamma_N \sum_{m=1}^{M} c_{mk} \sqrt{\eta_{mk}\gamma_{mk}} \right)^2 \Bigg). \qquad (32)
\end{aligned}$$

Now, if $m = m'$, we compute the expectation as

$$\begin{aligned}
&\mathbb{E}\left\{ \frac{\hat{\boldsymbol{g}}_{mk}^H}{\|\hat{\boldsymbol{g}}_{mk}\|_2} \left(\hat{\boldsymbol{g}}_{mk} + \boldsymbol{\epsilon}_{mk} \right) \left(\hat{\boldsymbol{g}}_{mk}^H + \boldsymbol{\epsilon}_{mk}^H \right) \frac{\hat{\boldsymbol{g}}_{mk}}{\|\hat{\boldsymbol{g}}_{mk}\|_2} \right\} \\
&= \mathbb{E}\left\{ \frac{\hat{\boldsymbol{g}}_{mk}^H \hat{\boldsymbol{g}}_{mk} \hat{\boldsymbol{g}}_{mk}^H \hat{\boldsymbol{g}}_{mk}}{\|\hat{\boldsymbol{g}}_{mk}\|_2^2} \right\} + \mathbb{E}\left\{ \frac{\hat{\boldsymbol{g}}_{mk}^H}{\|\hat{\boldsymbol{g}}_{mk}\|_2} \boldsymbol{\epsilon}_{mk} \boldsymbol{\epsilon}_{mk}^H \frac{\hat{\boldsymbol{g}}_{mk}}{\|\hat{\boldsymbol{g}}_{mk}\|_2} \right\} \\
&= \mathbb{E}\left\{ \hat{\boldsymbol{g}}_{mk}^H \hat{\boldsymbol{g}}_{mk} \right\} + \mathbb{E}\left\{ \frac{\hat{\boldsymbol{g}}_{mk}^H}{\|\hat{\boldsymbol{g}}_{mk}\|_2} \mathbb{E}\left\{ \boldsymbol{\epsilon}_{mk} \boldsymbol{\epsilon}_{mk}^H \right\} \frac{\hat{\boldsymbol{g}}_{mk}}{\|\hat{\boldsymbol{g}}_{mk}\|_2} \right\} \\
&= N\gamma_{mk} + \beta_{mk} - \gamma_{mk} = \beta_{mk} + (N-1)\gamma_{mk}. \qquad (33)
\end{aligned}$$

If $m \neq m'$, due to the independence between $\hat{\boldsymbol{g}}_{mk}$ and $\hat{\boldsymbol{g}}_{m'k}$, it holds

$$\mathbb{E}\left\{ \|\hat{\boldsymbol{g}}_{mk}\|_2 \right\} \mathbb{E}\left\{ \|\hat{\boldsymbol{g}}_{m'k}\|_2 \right\} = \Gamma_N^2 \sqrt{\gamma_{mk}\gamma_{m'k}}. \qquad (34)$$

Plugging (33) and (34) into (32) gives (23).

C. Computation of $\mathbb{E}\left\{|UI_{kk'}|^2\right\}$ with NCB precoding

$$\begin{aligned}
&\mathbb{E}\left\{ |\mathrm{UI}_{kk'}|^2 \right\} = \rho_d \mathbb{E}\left\{ |\boldsymbol{\varpi}_{k'}^{\mathrm{NCB}} \boldsymbol{g}_k|^2 \right\} \\
&= \rho_d \sum_{m=1}^{M} \sum_{m'=1}^{M} c_{mk'} c_{m'k'} \sqrt{\eta_{mk'}\eta_{m'k'}} \\
&\quad \times \mathbb{E}\left\{ \frac{\hat{\boldsymbol{g}}_{mk'}^H}{\|\hat{\boldsymbol{g}}_{mk'}\|_2} \boldsymbol{g}_{mk} \boldsymbol{g}_{m'k}^H \frac{\hat{\boldsymbol{g}}_{m'k'}}{\|\hat{\boldsymbol{g}}_{m'k'}\|_2} \right\} \\
&= \rho_d \sum_{m=1}^{M} c_{mk'}^2 \eta_{mk'} \underbrace{\mathbb{E}\left\{ \frac{\hat{\boldsymbol{g}}_{mk'}^H}{\|\hat{\boldsymbol{g}}_{mk'}\|_2} \boldsymbol{g}_{mk} \boldsymbol{g}_{mk}^H \frac{\hat{\boldsymbol{g}}_{mk'}}{\|\hat{\boldsymbol{g}}_{mk'}\|_2} \right\}}_{T_1} \\
&\quad + \rho_d \sum_{m=1}^{M} \sum_{m' \neq m}^{M} c_{mk'} c_{m'k'} \sqrt{\eta_{mk'}\eta_{m'k'}} \\
&\quad \times \underbrace{\mathbb{E}\left\{ \frac{\hat{\boldsymbol{g}}_{mk'}^H}{\|\hat{\boldsymbol{g}}_{mk'}\|_2} \boldsymbol{g}_{mk} \right\} \mathbb{E}\left\{ \boldsymbol{g}_{m'k}^H \frac{\hat{\boldsymbol{g}}_{m'k'}}{\|\hat{\boldsymbol{g}}_{m'k'}\|_2} \right\}}_{T_2}. \qquad (35)
\end{aligned}$$

Now, if $\varphi_{k'} = \varphi_k$ then $\hat{\boldsymbol{g}}_{mk'} = \frac{\beta_{mk'}}{\beta_{mk}} \hat{\boldsymbol{g}}_{mk}$, and we compute T_1 and T_2 as in (33) and (34), respectively. If $\varphi_{k'} \neq \varphi_k$, instead we have $T_2 = 0$ and

$$T_1 = \mathbb{E}\left\{ \frac{\hat{\boldsymbol{g}}_{mk'}^H}{\|\hat{\boldsymbol{g}}_{mk'}\|_2} \mathbb{E}\left\{ \boldsymbol{g}_{mk} \boldsymbol{g}_{mk}^H \right\} \frac{\hat{\boldsymbol{g}}_{mk'}}{\|\hat{\boldsymbol{g}}_{mk'}\|_2} \right\} = \beta_{mk}. \qquad (36)$$

Plugging T_1 and T_2 for both cases in (35) gives (24).

REFERENCES

[1] H. Q. Ngo, A. Ashikhmin, H. Yang, E. G. Larsson, and T. L. Marzetta, "Cell-Free Massive MIMO Versus Small Cells," *IEEE Transactions on Wireless Communications*, vol. 16, no. 3, pp. 1834–1850, March 2017.

[2] T. L. Marzetta, E. G. Larsson, H. Yang, and H. Q. Ngo, *Fundamentals of Massive MIMO*. Cambridge University Press, 2016.

[3] S. Buzzi and C. D'Andrea, "Cell-Free Massive MIMO: User-Centric Approach," *IEEE Wireless Communications Letters*, vol. 6, no. 6, pp. 706–709, Dec 2017.

[4] F. Riera-Palou, G. Femenias, A. G. Armada, and A. Pérez-Neira, "Clustered Cell-Free Massive MIMO," in *Proc. 2018 IEEE Globecom Workshops (GC Wkshps)*, Dec 2018, pp. 1–6.

[5] E. Björnson, J. Hoydis, and L. Sanguinetti, "Massive MIMO networks: Spectral, energy, and hardware efficiency," *Foundations and Trends® in Signal Processing*, vol. 11, no. 3-4, pp. 154–655, 2017. [Online]. Available: http://dx.doi.org/10.1561/2000000093

[6] Z. Chen and E. Björnson, "Channel Hardening and Favorable Propagation in Cell-Free Massive MIMO With Stochastic Geometry," *IEEE Transactions on Communications*, vol. 66, no. 11, pp. 5205–5219, Nov 2018.

[7] G. Interdonato, H. Q. Ngo, E. G. Larsson, and P. Frenger, "On the Performance of Cell-Free Massive MIMO with Short-Term Power Constraints," in *Proc. 2016 IEEE 21st International Workshop on Computer Aided Modelling and Design of Communication Links and Networks (CAMAD)*, Oct 2016, pp. 225–230.

[8] E. Björnson and L. Sanguinetti, "Making Cell-Free Massive MIMO Competitive With MMSE Processing and Centralized Implementation," *IEEE Transactions on Wireless Communications*, vol. 19, no. 1, pp. 77–90, Jan 2020.

[9] G. Femenias and F. Riera-Palou, "Cell-Free Millimeter-Wave Massive MIMO Systems With Limited Fronthaul Capacity," *IEEE Access*, vol. 7, pp. 44 596–44 612, 2019.

[10] M. Attarifar, A. Abbasfar, and A. Lozano, "Modified Conjugate Beamforming for Cell-Free Massive MIMO," *IEEE Wireless Communications Letters*, pp. 1–1, 2019.

[11] A. A. I. Ibrahim, A. Ashikhmin, T. L. Marzetta, and D. J. Love, "Cell-free massive MIMO systems utilizing multi-antenna access points," in *2017 51st Asilomar Conference on Signals, Systems, and Computers*, Oct 2017, pp. 1517–1521.

[12] R. S. Panwar and K. M. Sivalingam, "Implementation of wrap around mechanism for system level simulation of LTE cellular networks in NS3," in *Proc. 2017 IEEE 18th International Symposium on A World of Wireless, Mobile and Multimedia Networks (WoWMoM)*, June 2017, pp. 1–9.